Med Biol Eng Comput (2018) 56:635–648
DOI 10.1007/s11517-017-1709-8

ORIGINAL ARTICLE

MR image reconstruction via guided filter

Heyan Huang[1] · **Hang Yang**[2] · **Kang Wang**[3]

Received: 10 January 2017 / Accepted: 9 August 2017 / Published online: 25 August 2017

Abstract Magnetic resonance imaging (MRI) reconstruction from the smallest possible set of Fourier samples has been a difficult problem in medical imaging field. In our paper, we present a new approach based on a guided filter for efficient MRI recovery algorithm. The guided filter is an edge-preserving smoothing operator and has better behaviors near edges than the bilateral filter. Our reconstruction method is consist of two steps. First, we propose two cost functions which could be computed efficiently and thus obtain two different images. Second, the guided filter is used with these two obtained images for efficient edge-preserving filtering, and one image is used as the guidance image, the other one is used as a filtered image in the guided filter. In our reconstruction algorithm, we can obtain more details by introducing guided filter. We compare our reconstruction algorithm with some competitive MRI reconstruction techniques in terms of PSNR and visual quality. Simulation results are given to show the performance of our new method.

Keywords Image reconstruction · Magnetic resonance imaging · Compressive sensing · Guided filter

1 Introduction

Medical image processing is routinely applied for assessment and diagnosis of some diseases [1, 2], so the quality of the imaging will affect the accuracy of the diagnosis. Reconstruction of imagery from an incomplete set of samples from a Fourier representation is an significant target to improve scanning technologies, for instance, magnetic resonance imaging (MRI), computed tomography (CT). Solutions to such a problem would allow significant reductions in collection times and improve the quality of the images. One of the major challenges is the ill-posed nature of the reconstruction process due to insufficient measurements [3].

1.1 Problem description

Let $u \in \mathcal{C}^R$ denote an image to be reconstructed, and $f \in \mathcal{C}^m$ $(m < R)$ denote the undersampled Fourier measurements. They have the following relations $P\mathcal{F}u = f$, here, $\mathcal{F}$ represents the Fourier transform matrix, $P \in \mathcal{C}^{m\times R}$ is a "row selector" matrix, which comprises a subset of the rows of an identity matrix.

Compressed sensing (CS) could reconstruct the unknown image u from the measurements f by solving the underdetermined equation $P\mathcal{F}u = f$. Applying the sparsity constraint, the CS obtains the reconstructed image by minimizing the L_0 quasi norm of the sparsified image Ψu, where $\Psi \in \mathcal{C}^{T\times R}$ denotes a orthonormal sparsifying transform for the image u. The corresponding optimization problem is

$$\min_u \|\Psi u\|_0 \;\; s.t. \;\; P\mathcal{F}u = f \tag{1}$$

It is well known that this L_0 problem is a nondeterministic polynomial-time hard (NP-hard) problem. However, the greedy algorithms could solve this problem such as orthogonal matching pursuit (OMP) [4].

✉ Heyan Huang
huanghy10@mails.jlu.edu.cn

[1] School of Sciences, Changchun University, Changchun 130012, China

[2] Changchun Institute of Optics, Fine Mechanics and Physics, Chinese Academy of Sciences, Changchun 130033, China

[3] China FAW Group Corporation R&D Center, Changchun 130011, China

The typical formulation of the compressed sensing magnetic resonance imaging (CSMRI) reconstruction problem uses the L_1 norm instead of L_0 quasi norm, and has the following formulation

$$\min_u \|P\mathcal{F}u - f\|_2^2 + \lambda\|\Psi u\|_1 \tag{2}$$

This problem formulation contains a global sparsity measure and an analytical sparsifying transform Ψ.

1.2 Related work

The theory of CS [3, 5–7] could recover images accurately by using significantly fewer measurements than the number of unknowns. It demonstrates that the signal could be reconstructed with high probability when utilize the sparsity in some domain. Compared with the signal space dimension, the sparsity constraint significantly reduces the size of the set of possible signals. With this sparsity constraint, the CS reconstruction process is usually formulated as a constrained optimization problem, and it can be solved by the nonlinear algorithms or greedy algorithms [3–5, 8]. A variety of MRI reconstruction algorithms have achieved good results recently with the compressed sensing, such as static dynamic MRI [9, 10], MRI [11–13], and diffusion tensor imaging (DTI) [14]. In our paper, we mainly discuss the CS for static MRI.

In these MRI reconstruction algorithms, the total variation (TV) regularization [3, 15–18] is commonly used for image reconstruction. The TV regularization could obtain high reconstruction images due to its well desirable properties such as simplicity and edge-preserving ability. However, the TV regularization finds solution with sparse gradients, and may result in blocky effects when the measurements are undersampled [19]. Patel et al. [13] developed the algorithm called GradientRec to estimate the original image by recovering the horizontal and vertical gradients separately. This algorithm could obtain better recovery image quality compared with the method (called RecPF) proposed in [16]. In the RecPF method, the signals are reconstructed as minimizers of the sum of three terms corresponding to total variation, L_1-norm of a certain transform, and least squares data fitting. Recently, the extension of TV regularization has attracted much attention [20–22].

On the other hand, images with a sparse representation can be reconstructed from randomly undersampled data in the sparse transform domain. In the paper [11], the practical incoherent undersampling schemes are presented and analyzed by means of their aliasing interference. The MR reconstruction algorithm (called SparseMRI) in paper [11] is performed by minimizing the L_1 norm of a transformed image, subject to data fidelity constraints. The L_1 wavelet-based reconstruction algorithm tends to slightly shrink the magnitude of the reconstructed sparse coefficients and may appear small high-frequency oscillatory artifacts in the reconstruction. These artifacts are mitigated by adding a small TV penalty on top of the wavelet penalty in the SparseMRI reconstruction algorithm. In recent years, the adaptive transforms (dictionaries) based image reconstruction algorithms have become a research hotspot due to its fine properties. In these studies, the patch-based dictionaries [12, 23–26] could capture local image features effectively, remove noise and aliasing artifacts effectively in compressive sensing MRI (CSMRI) [27]. For a given fixed basis (finite difference, wavelet, etc.), it might not be universally optimal for all images [27]. The dictionary learning (DL) strategy reduces this drawback, and it assumes that each image patch is encoded with sparse coefficients utilizing an over-complete dictionary. But, this problem may be complicated due to the non-convexity and non-linearity [28]. One of the state-of-the-art DL methods for MR image recovery is the DLMRI algorithm [12], it learned the image-patch dictionary from a small number of samples and was proven to be very effective in reconstruction. The paper [29] proposed the MRI recovery algorithm by exploiting sparsity and low-rank structure to remove the noise artifacts while significantly improve the recovery quality. The paper [30] presented a new gradient based dictionary learning method for image recovery. It effectively combined the total variation and dictionary learning technique to well maintain the local features in the gradient images.

1.3 Guided filter

The guided filter [31] is a general linear translation-variant filtering process, which includes a guidance image u_I, an filtering input image u_p, and an output image u. Both u_I and u_p are given beforehand, and they can be identical. The key assumption of the guided filter is a local linear model between the guidance image u_I and the output image u. Assuming that u is a linear transform of u_I in a window ω_k centered at the pixel i:

$$u(i) = a_k u_I(i) + b_k \tag{3}$$

where (a_k, b_k) are some linear coefficients assumed to be constant in a window ω_k, and they are given by

$$a_k = \frac{\frac{1}{|\omega|}\Sigma_{i\in\omega_k} u_I(i)u_p(i) - \bar{p}_k}{\sigma_k^2 + \epsilon} \tag{4}$$

$$b_k = \bar{p}_k - a_k\mu_k \tag{5}$$

where, ω_k is the kth kernel function window, $|\omega|$ is the number of pixels in ω_k, ϵ is a regularization parameter, μ_k and σ_k^2 are the mean and variance of u_p in ω_k.

However, the pixel i is involved in all the overlapping windows ω_k that covers i, so the filtering output $u(i)$ can be given by

$$u(i) = \bar{a}_i u_I(i) + \bar{b}_i \tag{6}$$

where $\bar{a}_i = \frac{1}{|\omega|}\sum_{k\in\omega_k} a_k$ and $\bar{b}_i = \frac{1}{|\omega|}\sum_{k\in\omega_k} b_k$ are the average coefficients of all windows overlapping i. More details can be found in [31].

We denote the Eq. 6 as $u = \textbf{guidefilter}(u_I, u_p, \omega, \epsilon)$.

1.4 Proposed algorithm

Most of conventional CS recovery approaches formulate the problem of reconstruction of imagery from an incomplete set of samples as a cost functional. And the cost functional includes a constraint term which is imposed by the raw measurement data and the L_1 norm of a sparse representation of the reconstructed image. However, the sparse representation is usually exploited by virtue of a set of fixed bases (e.g., discrete cosine transform (DCT), wavelet and curvelet) for the entirety of a signal, and can only work efficiently when the signal is super sparse, sometimes without deterministic performance guarantees, or may suffer from relatively high recovery complexity. In this work, we adopt a different approach to the problem of MR image reconstruction by exploiting guided filter [31]. Derived from a local linear model, guided filter generates the filtering output by considering the content of a guidance image. We first integrate this filter into an iterative compressed sensing method. First, two estimated images are obtained by the proposed two cost functions. One of them contains more details information and another contains less details. The former will be filtered and the later will work as the guidance image respectively in the second step. Second, the guided filter is applied to the output of the first step to reduce ring and refine the reconstruction result. Comparing with some state-of-the-art methods, the experimental results demonstrate that this algorithm can provide competitive and even better figures of merit.

1.5 Paper organization

In Section 2, we discuss details about the proposed reconstruction algorithm. Simulation results are presented in Section 3. The discussion and concluding remarks are presented in Sections 4 and 5 respectively.

2 Methods

In this work, we propose an iterative compressed sensing MR reconstruction algorithm via guided filter. The guided filter is a novel explicit edge-preserving image filter. In guided filter, the filtering output is locally a linear transform of the guidance image. So the guided filter does not suffer from the gradient reversal artifacts and has good edge-preserving smoothing properties like the bilateral filter. We adopt it to reconstruct more details and suppress artifacts effectively in our method.

Our algorithm is based on the following two steps in the reconstruction process. In the first step, we propose two cost functions:

$$u_I = \arg\min_u\{\lambda\|\nabla u - \nabla u_E\|_2^2 + \|P\mathcal{F}u - f\|_2^2\} \tag{7}$$

$$u_p = \arg\min_u\{\beta\|u - u_E\|_2^2 + \|P\mathcal{F}u - f\|_2^2\} \tag{8}$$

where u_E is a pre-estimated image,"∇" represents a gradient operator, and $\lambda > 0, \beta > 0$ are the regularization parameters.

Alternatively, we diagonalize derivative operators after Fast Fourier Transform(FFT) for speedup. These yield solutions in the Fourier domain (the relevant derivations are provided in the Appendix)

$$\mathcal{F}u_I = \frac{P^T f - \lambda\mathcal{F}\triangle\mathcal{F}u_E}{|P|^2 - \lambda\mathcal{F}\triangle\mathcal{F}^{-1}} \tag{9}$$

$$\mathcal{F}u_p = \frac{P^T f + \beta\mathcal{F}u_E}{|P|^2 + \beta} \tag{10}$$

where P^T represents the complex conjugate of P, $\triangle = -\nabla^T\nabla$, $\mathcal{F}^{-1}$ represents the inverse Fourier transform matrix . The plus, multiplication, and division are all component-wise operators.

After the Fourier shrinkage steps (see Eqs. 9 and 10), the image u_p contains the more details and more amplified artifacts than u_I. So, we choose u_p as the filtering image and u_I as the guidance image in the second step. In this way, we could recover some details and reduce the amplified artifacts. We integrated this filter into the reconstruction problem. It leads to a powerful reconstruction algorithm that produces high-quality results.

Moreover, the guided filter is a fast and non-approximate linear-time algorithm, whose computational complexity is independent of the filtering kernel size. It has an $O(N^2)$ time (N^2 is the number of pixels in the image) exact algorithm for both grayscale and color images.

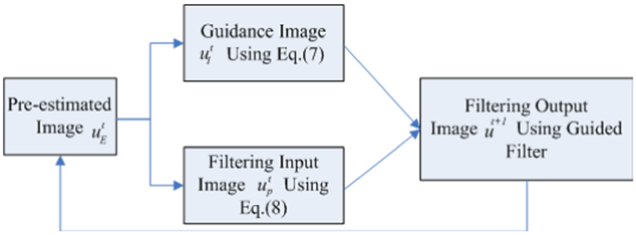

Fig. 1 Flowchart of our method

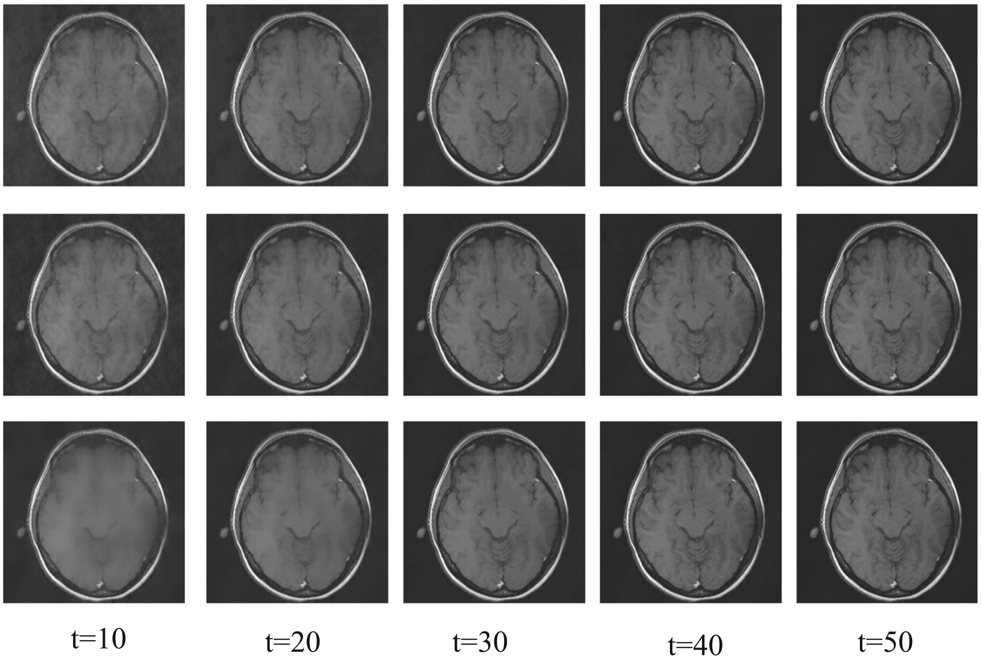
t=10 t=20 t=30 t=40 t=50

Fig. 2 Intermediate images u_I, u_p and the filtered output u_E with different iterations. The three rows denote the images u_I, u_p, and u_E with the number of iterations are 10, 20, 30, 40, 50, respectively

Figure 1 shows the flowchart of our proposed method. We summarize the proposed algorithm as follows:

Step 1: Set $t = 0$, pre-estimated image $u_E^t = 0$, choose guided filter parameters ω and ε.
Step 2: Use u_E^t to obtain the guidance image u_I^t and the filtering input image u_p^t with the Eqs. 7 and 8, respectively.
Step 3: Apply the guided filter to u_p^t with the guidance image u_I^t, and obtain a filtered output $u^{t+1} = \textbf{guidefilter}(u_I^t, u_p^t, \omega, \varepsilon)$.
Step 4: Set $u_E^t = u^{t+1}$, and $t = t + 1$.

back to Step 2.

As we claimed that u_p contains more details and artifacts than u_I, we choose u_p as the filtering image and u_I as the guidance image. To substantiate this statement and better understand the benefit of using the guided filter, we provide the intermediate images u_I^t, u_p^t and the filtered output u_E^{t+1} in Fig. 2, and the corresponding errors $u_E^{t+1} - u_I^t$ and $u_E^{t+1} - u_p^t$ in Fig. 3 with different iterations. From Fig. 2, we can see that the image texture of intermediate images u_I, u_p, and the filtered output u_E are becoming more and more rich with the iteration increases. Under the same number of iterations, u_p and u_E contains more details and artifacts than u_I. Figure 3 presents a better comparison between u_I and u_p. From this figure, we can see that the errors $u_E^{t+1} - u_I^t$ and $u_E^{t+1} - u_p^t$ are becoming smaller and smaller with the iteration increases, and the errors $u_E^{t+1} - u_I^t$ contains more details and artifacts than $u_E^{t+1} - u_p^t$ under the same iteration. That is to say, u_p contains more details and artifacts than u_I.

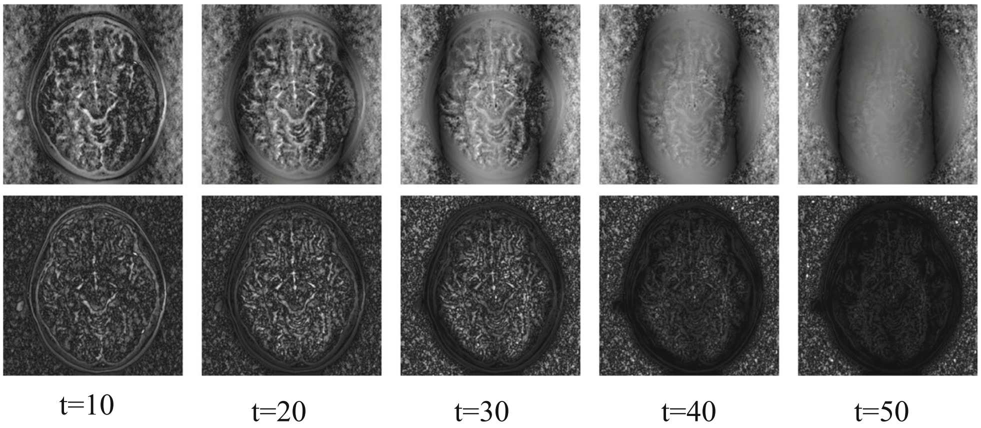
t=10 t=20 t=30 t=40 t=50

Fig. 3 The two rows represent the error images $u_E^{t+1} - u_I^t$ and $u_E^{t+1} - u_p^t$ with the number of iterations are 10, 20, 30, 40, 50, respectively

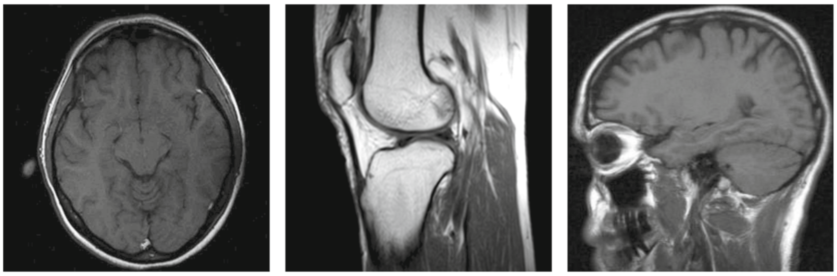

Fig. 4 Tested MR images

3 Results

In order to test the effectiveness of our algorithm, we have done several groups of experiments by a number of sampling schemes with different undersampling ratios. We implement our method in MATLAB on an Intel Core i5 CPU with 8 GB of RAM. Sampling schemes used in our experiments are produced in DLMRI toolbox, and they include 2D random sampling, cartesian sampling, pseudo radial sampling and low resolution sampling. The simulated data is obtained by undersampling the 2D DFT (discrete Fourier transform) of the MR images. In this section, we compare our method with the SparseMRI [11], TV+Waelet based RecPF [16] method, and the patch-based DLMRI [12] method. The MRI reconstruction quality is measured by the Peak Signal-to-Noise Ratio (PSNR). It is defined as

$$\mathrm{PSNR} = 20\log_{10}\frac{255}{\mathrm{RMSE}} \tag{11}$$

where RMSE is the root-mean-square error between the original image and the reconstructed image.

We consider different sampling schemes. In these experiments, the original images are Brain of size 512 × 512, Leg of size 512 × 512 and Head of size 512 × 512 (see Fig. 4). Table 1 summaries the different sampling schemes and sampling ratios.

In order to fairly compare the results, the regularization parameters (λ_1, λ_2) in RecPF and SparseMRI in each of the given experiment were hand tuned to show the best performance according to PSNR. The parameters of DLMRI method were set according to the default values [12].

Table 1 Description of the sampling schemes and sampling ratio for the eight experiments

	Sampling schemes	Sampling ratio
Exp.1	Random sampling pattern	5%
Exp.2	Random sampling pattern	10%
Exp.3	Pseudo radial sampling pattern	13.91%
Exp.4	Random sampling pattern	14.06%
Exp.5	Low resolution sampling pattern	14.06%
Exp.6	Pseudo radial pattern	16.41%
Exp.7	Cartesian sampling pattern	19.14%
Exp.8	Cartesian sampling pattern	25%

The parameters in our proposed method were hand tuned to get the best performance according to PSNR. For the parameter λ, we found that a larger value of it would result in a smooth image, whereas some details may lost. We have empirically found that $\lambda \in [10^{-4}, 10^{-5}]$, $\beta \in [10^{-4}, 10^{-5}]$ generally yields good results and we used 6×10^{-5}, 8×10^{-5} for the results in the experiments, respectively. Parameters ϵ and ω of guided filter should be set carefully. For this work, we have just tried to evaluate how robust the algorithm behaves for two different images and a wide range of image compression. We have empirically found that large ϵ and ω would obtain better recovery result for the low sampling ratio, and smaller ϵ and ω are suitable for the high sampling ratio. We have hand-optimized the two parameters with different sampling schemes and three different images for good results, obtaining $\epsilon \in [0.001, 0.01]$ and $\omega \in [2, 10]$.

In order to validate the effectiveness of our algorithm, we have compared the proposed method with three state-of-the-art algorithms: SparseMRI [11], RecPF [16], DLMRI [12] in different sampling schemes settings and different images. Tables 2, 3, and 4 display the PSNRs of reconstructed image by four methods with different sampling schemes for brain image, leg image, and head image respectively. From these numerical performances, we can see that our method clearly outperforms the other methods.

Figure 5 shows the visual comparison of brain reconstructions employing 2D variable density random sampling

Table 2 PSNR (in dB) of different methods for brain image

Experiments	RecPF	SparseMRI	DLMRI	Our method
Exp.1	36.72	30.01	35.72	*38.76*
Exp.2	41.36	32.79	40.59	*43.44*
Exp.3	38.04	33.36	37.52	*39.49*
Exp.4	39.60	32.64	39.27	*42.65*
Exp.5	33.08	31.92	34.73	*34.83*
Exp.6	39.31	33.62	38.88	*41.70*
Exp.7	40.98	34.28	41.26	*43.19*
Exp.8	42.92	35.93	42.53	*45.22*

Data in italics present the highest PSNR results with each experiment in the four methods

Table 3 PSNR (in dB) of different methods for leg image

Experiments	RecPF	SparseMRI	DLMRI	Our method
Exp.1	34.13	21.59	30.88	*35.75*
Exp.2	42.48	30.45	43.54	*48.23*
Exp.3	38.31	28.05	39.01	*41.07*
Exp.4	38.55	27.04	35.69	*43.08*
Exp.5	35.38	29.81	37.01	*37.27*
Exp.6	40.01	29.30	40.48	*43.20*
Exp.7	42.35	31.98	45.04	*46.31*
Exp.8	44.74	33.06	46.94	*49.23*

Data in italics present the highest PSNR results with each experiment in the four methods

with the sampling ration is 5% (Exp.1). The PSNRs of the reconstructions using zero-filled, RecPF, SparseMRI, DLMRI, and our method are 22.24 dB, 36.71 dB, 30.01 dB, 35.71 dB and 38.76 dB, respectively. Subfigures Fig. 5b, c, and g show the performance of zero-filled, RecPF and SparseMRI methods. We can see that some of the artifacts are maintained in the zero-filled reconstruction, and the results of RecPF and SparseMRI could not suppress undesirable artifacts and loses many details. That is the RecPF and SparseMRI only exploits the sparsity in wavelet domain and finite difference domain instead of adaptable domain, which is sufficient to represent the complex components inherent in the image. Instead, the dictionary learning (DLMRI) (Fig. 5h) obtain better reconstruction, and the results are seen to have lesser artifacts. Compared to zero-filled, SparseMRI, RecPF, and DLMRI methods, the reconstruction result and errors in subfigures Fig. 5i, l show that our method have succeeded in removing most of artifacts without sacrificing resolution. The error images of zero-filled, DLMRI, RecPF, and SparseMRI in Fig. 5e, f, j, k are seen to have more visible structures than our method.

Table 4 PSNR (in dB) of different methods for head image

Experiments	RecPF	SparseMRI	DLMRI	Our method
Exp.1	31.86	24.32	28.18	*33.18*
Exp.2	37.08	28.73	36.06	*38.45*
Exp.3	36.49	31.86	36.17	*38.15*
Exp.4	34.22	27.19	29.63	*35.46*
Exp.5	33.63	31.88	34.52	*34.60*
Exp.6	38.22	33.07	37.22	*39.46*
Exp.7	38.03	34.48	38.96	*39.91*
Exp.8	39.68	35.80	40.00	*41.56*

Data in italics present the highest PSNR results with each experiment in the four methods

Figure 6 shows the brain (512 × 512) image reconstruction results of our method with 2D Cartesian sampling (Exp.7). The sampling scheme showing in Fig. 6d can be found in [12]. The k-space was undersampled by randomly choosing phase-encode lines [12]. Subfigures Fig. 6b, c, g, h are the zero-filled, RecPF, SparseMRI, and DLMRI reconstructions, respectively, and subfigures Fig. 6e, f, j, k, l are the magnitude of reconstruction errors for zero-filled, RecPF, SparseMRI, DLMRI, and our methods. By looking reconstruction and error results carefully, we can see that our method reconstruction in Fig. 6i preserves image features better, and it clearer than other methods.

Figure 7 shows the reconstruction and error results of different methods for leg image with pseudo radial sampling and the sampling ratio is 13.91% of the k-space data (Exp.3). By examining these figures, we can see that the corresponding regions in our proposed method reconstruction are clearer and sharper than other methods (Fig. 7i). The magnitude image of the reconstruction error indicates that our method obtains lower magnitude and less structure than DLMRI and RecPF methods (Fig. 7l). The PSNR of our method (41.07dB) was 2.76 dB higher than that of RecPF and 2.06 dB higher than that of DLMRI.

Figure 8 shows the reconstructed results of the leg image with Exp.6, and subfigures Fig. 8b, c, g, h, i represent the reconstruction results by zero-filled, RecPF, SparseMRI, DLMRI, and our method, respectively. The corresponding PSNRs are 31.99 dB, 40.00 dB, 29.30 dB , 40.48 dB, and 43.19 dB respectively. By looking carefully at the reconstructions, we can see that our method effectively suppress the artifacts. Subfigures Fig. 8e, f, j, k demonstrate that larger reconstruction errors are exhibited by zero-filled, RecPF, SparseMRI, and DLMRI methods but not our proposed method (Fig. 8l). Our method could provide better reconstruction results in generally, and can recover more fine details than DLMRI and RecPF methods.

MR image reconstruction results for head image with 2D random sampling and 5% sampling ration (Exp.1) are shown in Fig. 9, with images in Fig. 9b, c, g, h, i indicating the reconstruction results of zero-filled, RecPF, SparseMRI, DLMRI, and our method respectively. The corresponding PSNRs are 20.46 dB, 31.86 dB, 24.32 dB, 28.18 dB, and 33.18 dB respectively. From these figures, we can see that our method effectively suppresses the artifacts but not zero-filled, SparseMRI and DLMRI. Figure 9e, f, j, k, l demonstrate that our proposed method exhibits less reconstruction errors than other four methods.

In Fig. 10, we show some experimental results of Exp.1 for brain image to demonstrate the convergence behavior of the proposed algorithm. We plot the cost value as a function of iteration for the cost functions Eqs. 7 and 8 in the left side of the Fig. 10. From the left curves, we can see that the

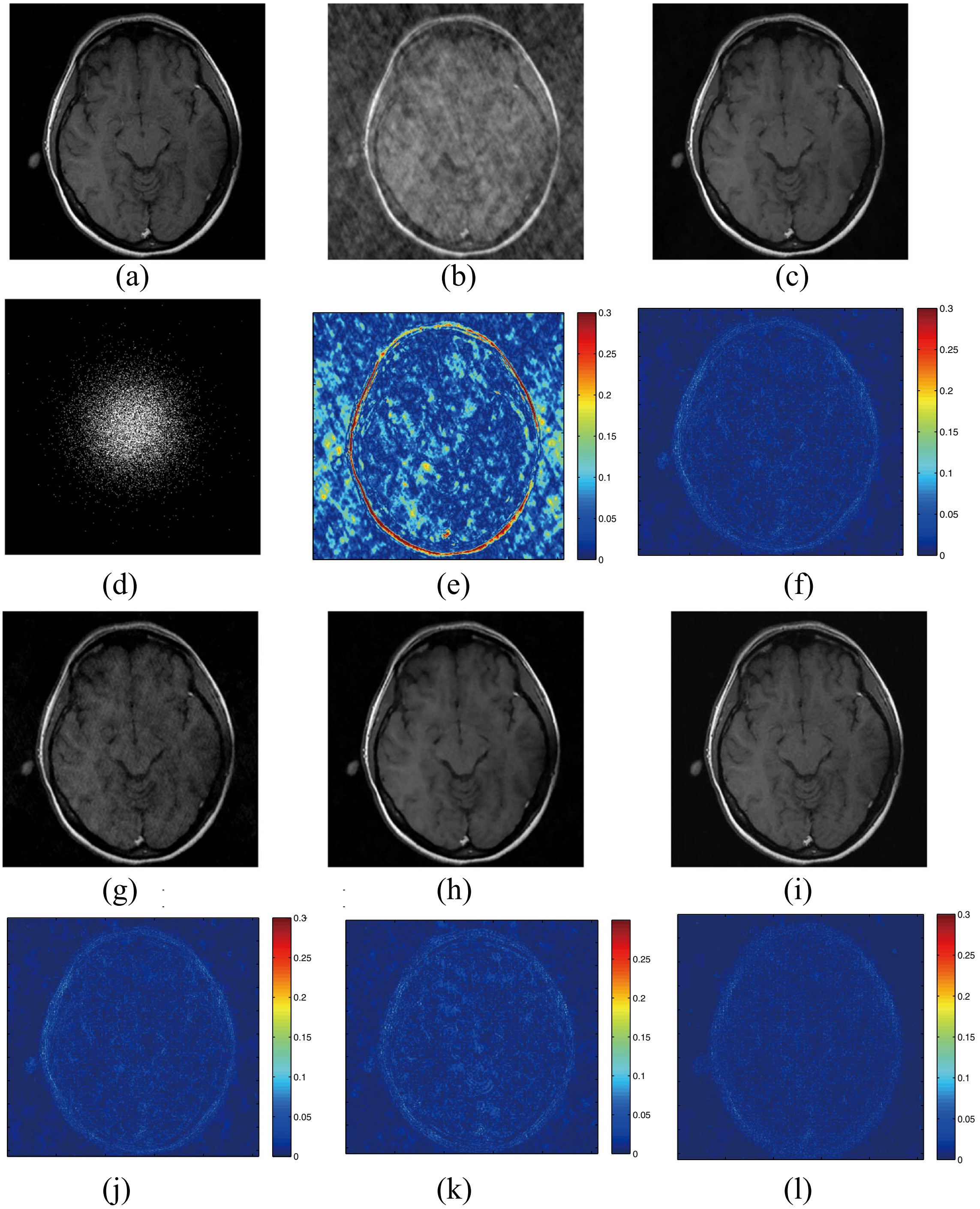

Fig. 5 Visual comparison of brain reconstructions using different methods with 20% undersampling (Exp.1). **a** Reference image, **b** zero-filled reconstruction, **c** RecPF reconstruction, **d** sampling mask in k-space with 20% undersampling, **e** magnitude of reconstruction error for (**b**), **f** magnitude of reconstruction error for (**c**), **g** SparseMRI reconstruction, **h** DLMRI reconstruction, **i** reconstruction using our proposed method, **j** magnitude of reconstruction error for (**g**), **k** magnitude of reconstruction error for (**h**), **l** magnitude of reconstruction error for (**i**)

cost values of Eqs. 7 and 8 decrease as the number of iteration increases. In order to better explain the convergence of our method, we plot the curve in the right of Fig. 10, which denotes the ratio of L_2-norm of the errors between the reconstructed image u^{t+1} and the original image u at each iteration with the original image (that is, the value of $\frac{\|u^{t+1}-u\|_2}{\|u\|_2}$). With the increase of iterations, we can see that the ration is getting smaller and smaller compared with

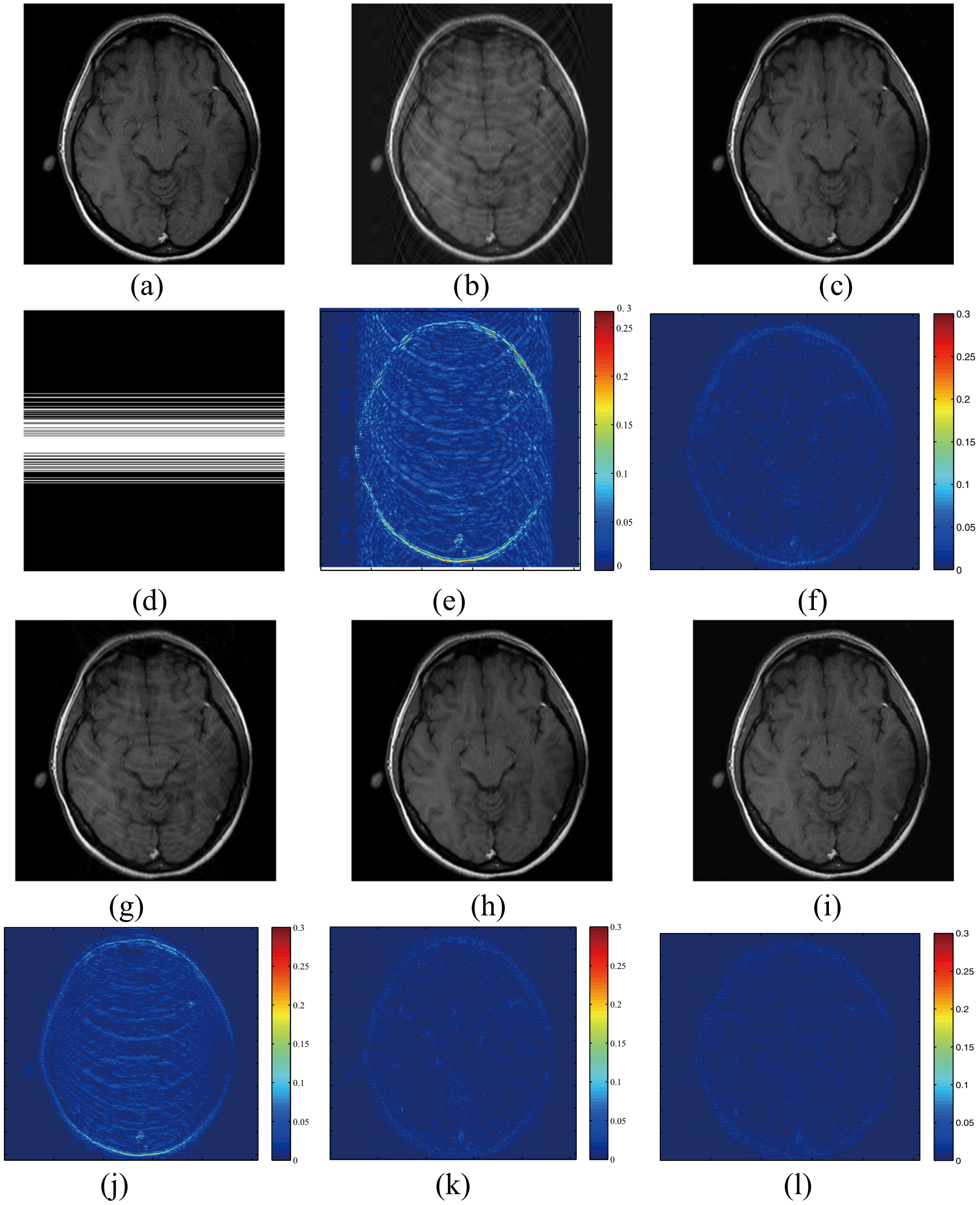

Fig. 6 Visual comparison of brain reconstructions using different methods with 19.14% undersampling (Exp.7). **a** Reference image, **b** zero-filled reconstruction, **c** RecPF reconstruction, **d** sampling mask in k-space with 19.14% undersampling, **e** magnitude of reconstruction error for (**b**), **f** magnitude of reconstruction error for (**c**), **g** SparseMRI reconstruction, **h** DLMRI reconstruction, **i** reconstruction using our proposed method, **j** magnitude of reconstruction error for (**g**), **k** magnitude of reconstruction error for (**h**), **l** magnitude of reconstruction error for (**i**)

the original image, that is to say the reconstructed image approaches the original image as the number of iteration increases. So whenever this ratio achieves a certain level, we terminate the iteration.

4 Discussion

The MRI reconstruction from an incomplete of Fourier samples is an significant target to improve scanning technologies,

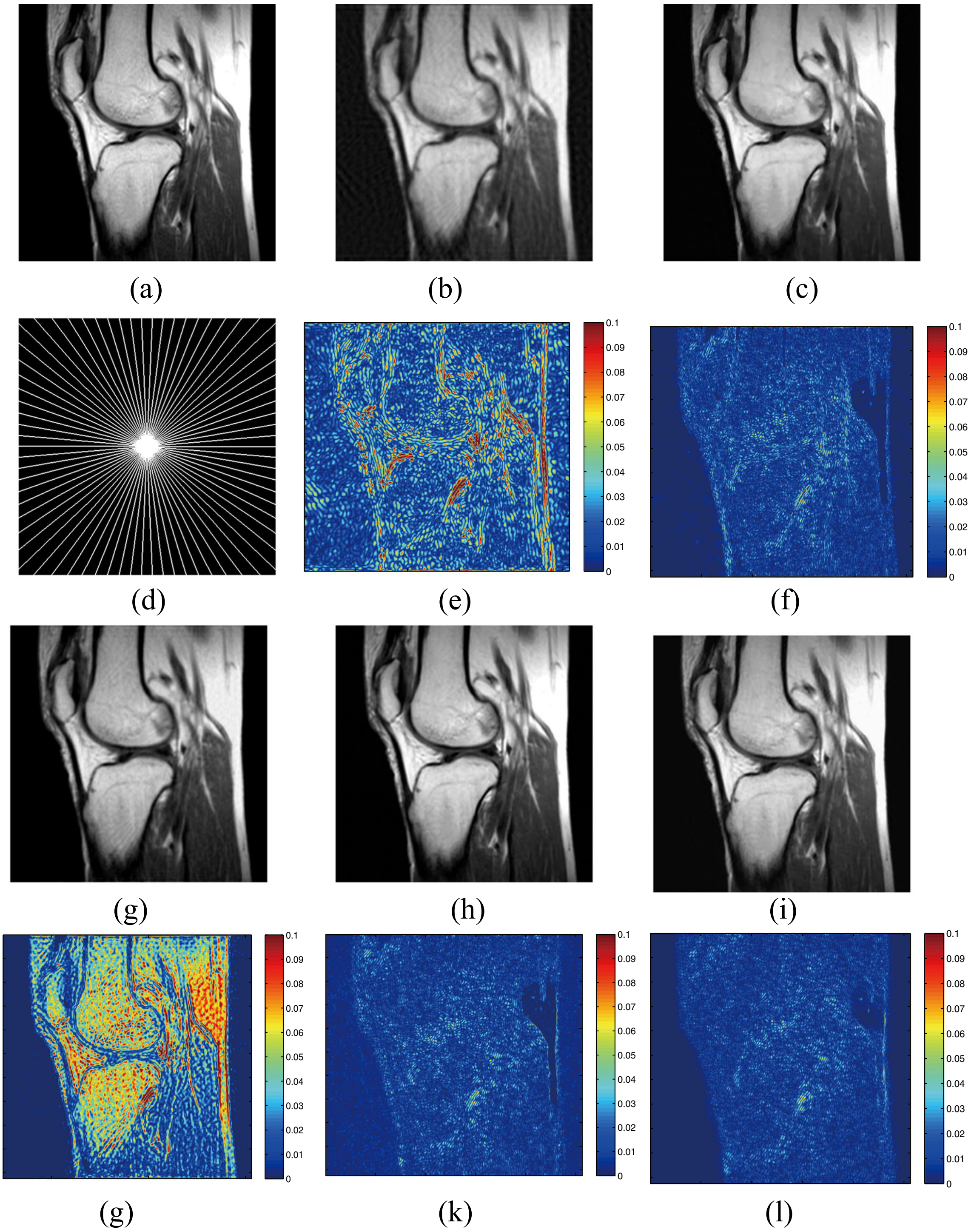

(a) (b) (c)

(d) (e) (f)

(g) (h) (i)

(g) (k) (l)

Fig. 7 MR image reconstruction results of our method for leg image with pseudo radial sampling (Exp.3). **a** Reference image, **b** zero-filled reconstruction, **c** RecPF reconstruction, **d** sampling mask in k-space with 20% undersampling, **e** magnitude of reconstruction error for (**b**), **f** magnitude of reconstruction error for (**c**), **g** SparseMRI reconstruction, **h** DLMRI reconstruction, **i** reconstruction using our proposed method, **j** magnitude of reconstruction error for (**g**), **k** magnitude of reconstruction error for (**h**), **l** magnitude of reconstruction error for (**i**)

and it can quickly carry out accurate and safe examination reports for doctors with high quality images. As well known, one of the major challenges is the ill-posed nature of the reconstruction process due to insufficient samples. The theory of CS could reconstruct the unknown image by using significantly fewer measurements than the number

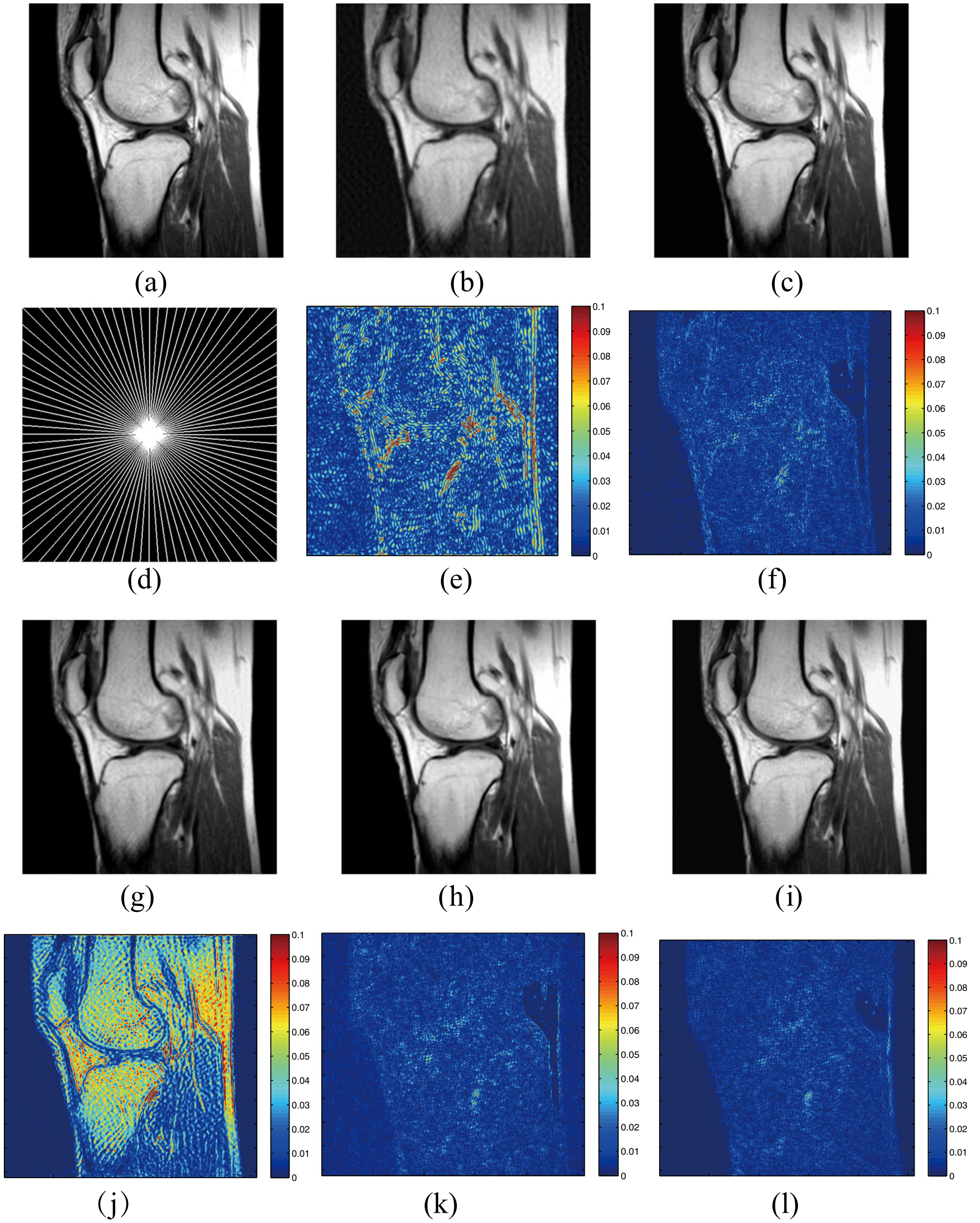

Fig. 8 Visual comparison of leg reconstructions using different methods with 16.41% undersampling (Exp.6). **a** Reference image, **b** zero-filled reconstruction, **c** RecPF reconstruction, **d** sampling mask in k-space with 16.14% undersampling, **e** magnitude of reconstruction error for (**b**), **f** magnitude of reconstruction error for (**c**), **g** SparseMRI reconstruction, **h** DLMRI reconstruction, **i** reconstruction using our proposed method, **j** magnitude of reconstruction error for (**g**), **k** magnitude of reconstruction error for (**h**), **l** magnitude of reconstruction error for (**i**)

of unknowns, and some MRI reconstruction algorithms with the compressed sensing have proved to be successful [12, 13, 16, 27]. In this paper, our primary objective is to present an effective MRI reconstruction algorithm with high quality images. Unlike the conventional CS reconstruction approaches with a cost functional, our MRI reconstruction

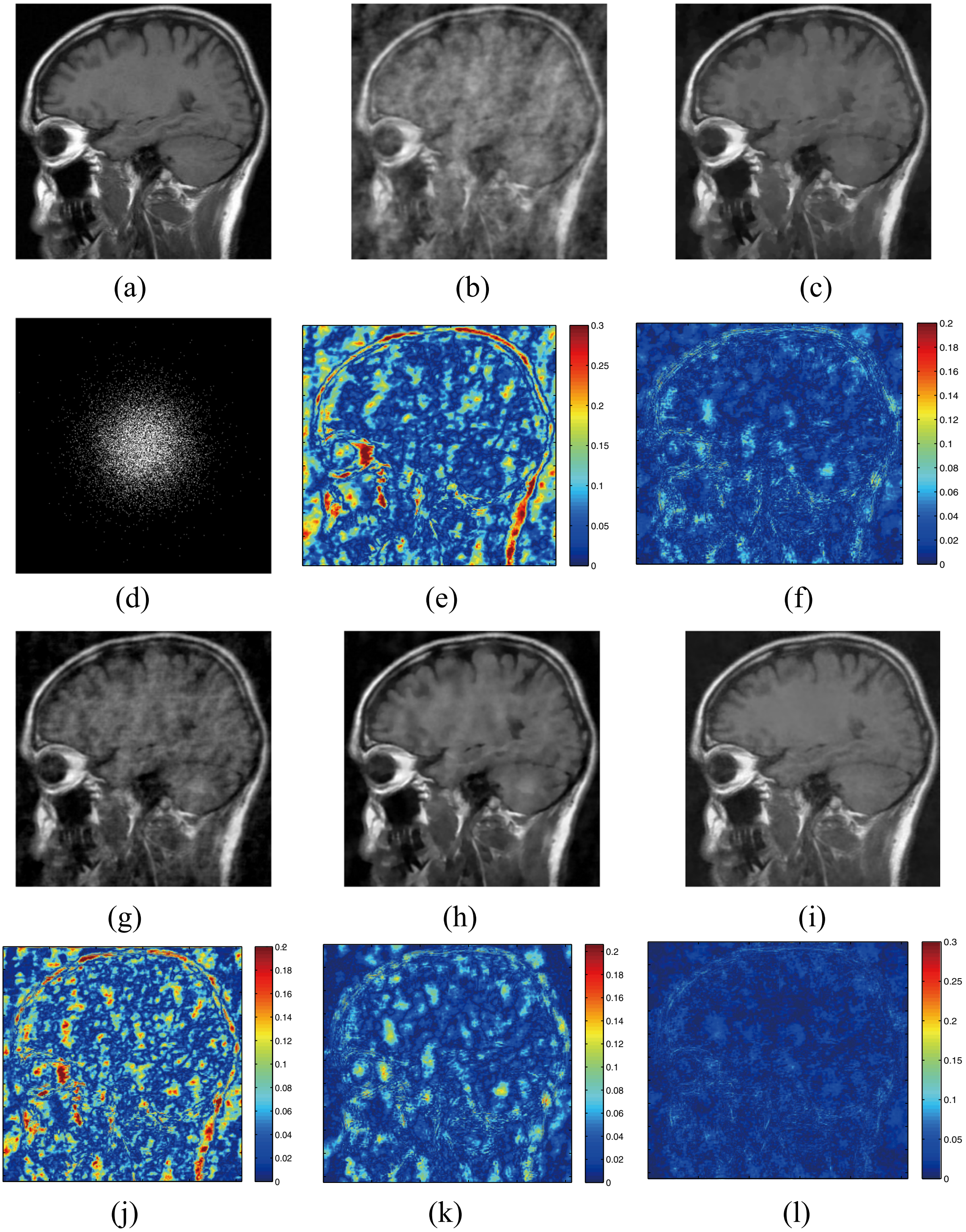

Fig. 9 MR image reconstruction results of our method for head image with 2D random sampling (Exp.1). **a** Reference image, **b** zero-filled reconstruction, **c** RecPF reconstruction, **d** sampling mask in k-space with 20% undersampling, **e** magnitude of reconstruction error for (**b**), **f** magnitude of reconstruction error for (**c**), **g** SparseMRI reconstruction, **h** DLMRI reconstruction, **i** reconstruction using our proposed method, **j** magnitude of reconstruction error for (**g**), **k** magnitude of reconstruction error for (h), **l** magnitude of reconstruction error for (**i**)

process can be divided into two steps: first, we propose two cost functions to obtain two estimated images with different information; second, we incorporate the guided filter into the MRI reconstruction process, the former two estimated images, with one as the guidance image and the other as the filtering image, then the guided filter is applied to reduce ring and refine the result of filtering image.

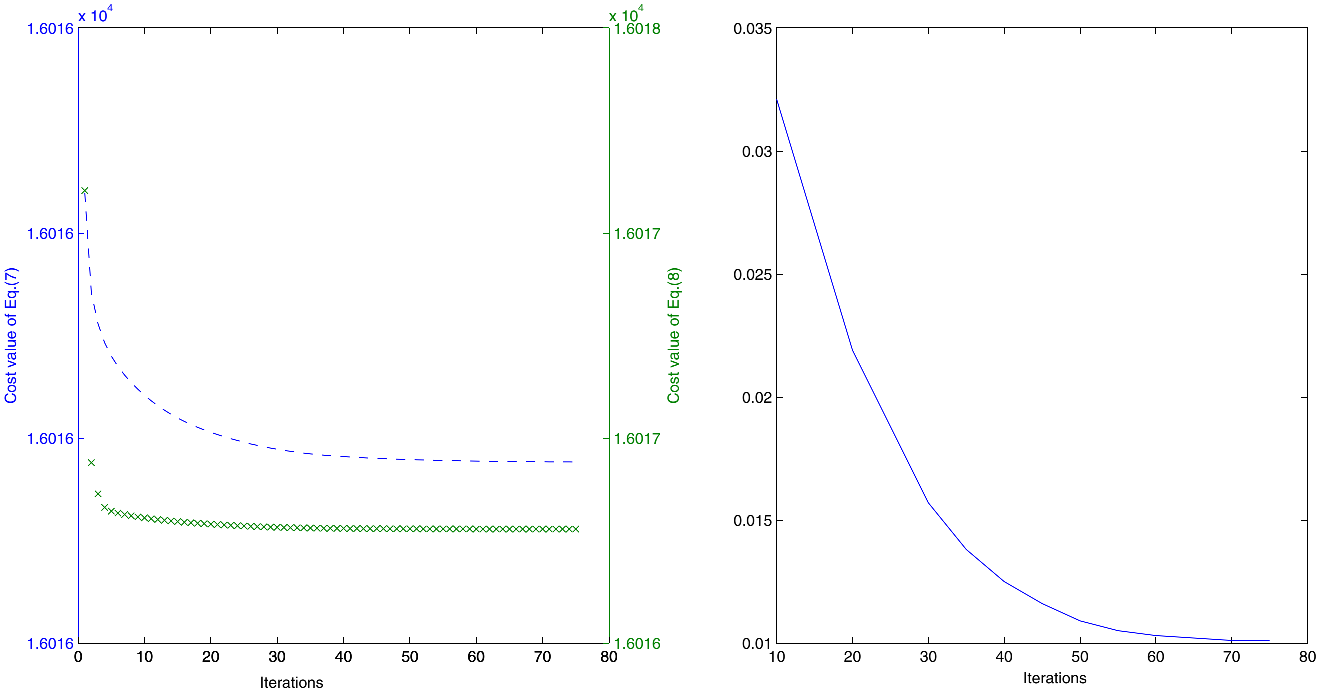

Fig. 10 Left: The cost values of iteration for equations (7)("–") and (8)("×"). Right: The value of $\frac{\|u^{t+1}-u\|_2}{\|u\|_2}$ at each iteration

In the experimental section, we have shown several groups of results by a number of sampling schemes with different undersampling ratios, and compared with other MRI reconstruction algorithms. From Figs. 5–9, Tables 2–4, we can see that our proposed method could obtain higher quality images under the same measurements. The better results of our method are mainly attributed to the following factors. First, we utilize the total variation in the proposed cost function (7) to obtain image u_I which could preserve the structure information of the original image with less details. The estimated image u_p from the proposed cost function (8) contains more details than u_I. The guided filter is an edge-preserving image filter, and it does not suffer from the gradient reversal artifacts. We utilize it to reconstruct more details and suppress artifacts effectively. The image u_p contains more details and more amplified artifacts then u_I. We adopt the u_I as the guidance image and u_p as the filtering image to recover more details and reduce the amplified artifacts.

The reconstruction of MRI without noise is mainly discussed in this paper. We will study the reconstruction of MR image with noise in the future.

5 Conclusion

In our work, we adopt a different approach to solve the problem of MRI reconstruction. The proposed method integrates the guided filter into an iterative image reconstruction method. In each iteration, the reconstruction process is divided into two steps. First, we obtain two images by the proposed two cost functions. The one will be filtered by the guided filter and the other one will work as the guidance image respectively. During the second step, the guided filter is applied to reduce ring and refine the result of the first step. Comparing with the some latest MRI reconstruction methods, we demonstrate with experimental results that this algorithm provides competitive and even better figures of merit.

Acknowledgments We would like to thank the anonymous reviewers for their helpful feedback. This research is supported by the National Science Foundation of China under Grant No. 61401425.

Appendix

The derivation from Eqs. 7 and 8 to Eqs. 9 and 10

We first must be precise about our notation. In the following, we have $\|\nabla u - \nabla u_E\|_2^2 = \|\nabla_x u - \nabla_x u_E\|_2^2 + \|\nabla_y u - \nabla_y u_E\|_2^2$, where ∇_x represents the horizontal difference operator, and ∇_y represents the vertical differential operator.

To find the optimal value of u_I, we must solve the optimization problem

$$u_I = \arg\min_u\{\lambda\|\nabla_x u - \nabla_x u_E\|_2^2 + \|\nabla_y u - \nabla_y u_E\|_2^2 + \|P\mathcal{F}u - f\|_2^2\} \tag{12}$$

Because this problem is differentiable, the optimality conditions for u_I are easily derived. By differentiating with respect to u and setting the result equal to zero, we get the update rule

$$\begin{aligned}&[\lambda(\nabla_x^T\nabla_x + \nabla_y^T\nabla_y) + \mathcal{F}^T P^T P\mathcal{F}]u \\ &\quad = \lambda(\nabla_x^T\nabla_x + \nabla_y^T\nabla_y)u_E + \mathcal{F}^T P^T f\end{aligned} \tag{13}$$

We now take advantage of the identities $\nabla^T\nabla = -\triangle$ and $\mathcal{F}^T = \mathcal{F}^{-1}$ to get

$$(\mathcal{F}^T P^T P\mathcal{F} - \lambda\triangle)u = \mathcal{F}^T P^T f - \lambda\triangle u_E \tag{14}$$

Therefore, the system that must be inverted to solve for u_I is circulant. Because of the circulant structure of this system, we can solve for the optimal value of u_I using only two Fourier transform. Through the Eq. 14, we can get the Eq. 9

$$\mathcal{F}u_I = \frac{P^T f - \lambda\mathcal{F}\triangle\mathcal{F}u_E}{|P|^2 - \lambda\mathcal{F}\triangle\mathcal{F}^{-1}} \tag{15}$$

Similarly, the problem (8) is differentiable. By differentiating with respect to u and setting the result equal to zero, we get the update rule

$$(\beta + \mathcal{F}^T P^T P\mathcal{F})u = \beta u_E + \mathcal{F}^T P^T f \tag{16}$$

which is

$$\mathcal{F}^T(\beta + P^T P)\mathcal{F}u = \mathcal{F}^T(\beta\mathcal{F}u_E + P^T f) \tag{17}$$

Thus, we can get the Eq. 10

$$\mathcal{F}u_p = \frac{P^T f + \beta\mathcal{F}u_E}{|P|^2 + \beta} \tag{18}$$

References

1. Zhang H, Li B, Young AA et al (2010) Recovery of myocardial kinematic function without the time history of external loads[J]. Eur J Advances Signal Process (1):1–9
2. Tavakoli V, Amini AA (2013) A survey of shaped-based registration and segmentation techniques for cardiac images[J]. Comp Vision Image Underst (CVIU) 117(9):966–989
3. Cands EJ, Romberg J, Tao T (2006) Robust uncertainty principles: Exact signal reconstruction from highly incomplete frequency information[J]. IEEE Trans Inf Theory 52(2):489–509
4. Tropp JA, Gilbert AC (2007) Signal recovery from random measurements via orthogonal matching pursuit[J]. IEEE Trans Inf Theory 53(12):4655–4666
5. Donoho DL (2006) Compressed sensing[J]. IEEE Trans Inf Theory 52(4):1289–1306
6. Cands EJ, Wakin MB (2008) An introduction to compressive sampling[J]. IEEE Signal Process Mag 25(2):21–30
7. Baraniuk RG (2007) Compressive sensing[J]. IEEE Signal Process Mag 24(4)
8. Needell D, Tropp JA (2009) CoSaMP: Iterative signal recovery from incomplete and inaccurate samples[J]. Appl Comput Harmon Anal 26(3):301–321
9. Lustig M, Santos JM, Donoho DL, Pauly JM (2006) kt SPARSE: High frame rate dynamic MRI exploiting spatio-temporal sparsity[C]. In: Proceedings of the 13th annual meeting of ISMRM, Seattle, p 2420
10. Gamper U, Boesiger P, Kozerke S (2008) Compressed sensing in dynamic MRI[J]. Magn Reson Med 59(2):365–373
11. Lustig M, Donoho D, Pauly JM (2007) Sparse MRI: The application of compressed sensing for rapid MR imaging[J]. Magn Reson Med 58(6):1182–1195
12. Ravishankar S, Bresler Y (2011) MR Image reconstruction from highly undersampled k-space data by dictionary learning[J]. IEEE Trans Med Imaging 30(5):1028–1041
13. Patel VM, Maleh R, Gilbert AC, Chellappa R (2012) Gradient-based image recovery methods from incomplete Fourier measurements[J]. IEEE Trans Image Process 21(1):94–105
14. Adluru G, DiBella EVR (2008) Reordering for improved constrained reconstruction from undersampled k-space data[J]. J Biomed Imaging vol 9
15. Ma S, Yin W, Zhang Y, Chakraborty A (2008) An efficient algorithm for compressed MR imaging using total variation and wavelets[C]. Computer Vision and Pattern Recognition, 2008. CVPR 2008. IEEE Conference on. IEEE, pp 1–8
16. Yang J, Zhang Y, Yin W (2010) A fast alternating direction method for $TVL_1 - L_2$ signal reconstruction from partial Fourier data[J]. IEEE J Sel Top Sign Proces 4(2):288–297
17. Liu B, King K, Steckner M, Xie J, Sheng J, Ying L (2009) Regularized sensitivity encoding (SENSE) reconstruction using Bregman iterations[J]. Magn Reson Med 61(1):145–152
18. Ramani S, Fessler JA (2011) Parallel MR image reconstruction using augmented Lagrangian methods[J]. IEEE Trans Med Imaging 30(3):694–706
19. Hu Y, Jacob M (2012) Higher degree total variation (HDTV) regularization for image recovery[J]. IEEE Trans Image Process 21(5):2559–2571
20. Elad M, Milanfar P, Rubinstein R (2007) Analysis versus synthesis in signal priors[J]. Inverse Prob 23(3):947
21. Nam S, Davies ME, Elad M, Gribonval R (2013) The cosparse analysis model and algorithms[J]. Appl Comput Harmon Anal 34(1):30–56
22. Giryes R, Nam S, Elad M, Gribonval R, Davies ME (2014) Greedy-like algorithms for the cosparse analysis model[J]. Linear Algebra Appl 441:22–60
23. Liang D, Wang H, Chang Y, Ying L (2011) Sensitivity encoding reconstruction with nonlocal total variation regularization[J]. Magn Reson Med 65(5):1384–1392
24. Egiazarian K, Foi A, Katkovnik V (2007) Compressed sensing image reconstruction via recursive spatially adaptive filtering[C]. 2007 IEEE International Conference on Image Processing. IEEE 1:I-549-I-552
25. Aharon M, Elad M, Bruckstein A (2006) K-SVD: An algorithm for designing overcomplete dictionaries for sparse representation[J]. IEEE Trans Signal Process 54(11):4311–4322
26. Li J, Song Y, Zhu Z et al (2016) Highly undersampled MR image reconstruction using an improved dual-dictionary learning method with self-adaptive dictionaries[J]. Medical & Biological Engineering & Computing pp 1–16
27. Qu X, Guo D, Ning B, Hou Y, Lin Y, Cai S, Chen Z (2012) Undersampled MRI reconstruction with patch-based directional wavelets[J]. Magn Reson Imaging 30(7):964–977
28. Skretting K, Engan K (2010) Recursive least squares dictionary learning algorithm[J]. IEEE Trans Signal Process 58(4):2121–2130
29. Yin XX, Ng BWH, Ramamohanarao K et al. (2012) Exploiting sparsity and low-rank structure for the recovery of multi-slice breast MRIs with reduced sampling error[J]. Med Biol Eng Comput 50(9):991–1000

30. Liu Q, Wang S, Ying L, Peng X, Zhu Y, Liang D (2013) Adaptive dictionary learning in sparse gradient domain for image recovery[J]. IEEE Trans Image Process 22(12):4652–4663
31. He K, Sun J, Tang X (2010) Guided image filtering[C]. European conference on computer vision. Springer Berlin Heidelberg, pp 1–14

Heyan Huang received her Doctor of Mathematics in 2013 from The University of Jilin. Now, she is a university lecturer of Changchun University. Her present research interests include image reconstruction, compressed sensing, image denoising and pattern recognition.

Hang Yang is working at Changchun Institute of Optics, Fine Mechanics and Physics, Chinese Academy of Science. His present research interests include image processing, compressed sensing, inverse problem and pattern recognition.

Kang Wang is working China FAW group corporation RD center, Changchun, China. His present research interests include pattern recognition and intelligent systems.